Elsevier Editorial System(tm) for Acta Materialia
Manuscript Draft

Manuscript Number: A-11-1721R2

Title: Structural and Magnetic Nano-clusters in Cu50Zr50-xGdx (x= 5 at%) Metallic Glasses

Article Type: Full Length Article

Keywords: metallic glasses; phase separation; atom-probe field ion microscopy; small-angle X-ray scattering; magnetic nanostructure

Corresponding Author: Dr. Norbert Mattern,

Corresponding Author's Institution:

First Author: Norbert Mattern

Order of Authors: Norbert Mattern; Ahmed Shariq; Bjorn Schwarz; Ulla Vainio; Jurgen Eckert

Abstract: It is shown that phase separated metallic glasses on the nanoscale can be prepared by rapid quenching of Cu50Zr50-xGdx melts with low concentration of gadolinium (x = 5 at%). Gd-enriched clusters of 2 nm size are formed as early stages of decomposition in the deeply undercooled melt. The key physical parameter to obtain such nano clustered microstructure upon quenching is the critical temperature of liquid-liquid phase separation which has to be close to the glass transition temperature. Thus, the thermodynamic properties of the liquid phase even in the metastable deeply under-cooled melt determine essentially the structure formation. Analysis of spatial atomic arrangement by atom probe tomography after annealing in the super-cooled liquid state gives direct evidence of the spinodal character of decomposition by up-hill diffusion. The Gd-enriched nano-clusters exhibit ferromagnetic ordering below 50 K and the cluster size regime derived from magnetization measurements is in good agreement with that obtained from atom probe tomography investigations. First stage of crystallization of Cu50Zr45Gd5 glass is observed to be Ostwald type ripening on a nanoscale. The phase separated glass acts as a precursor for the formation of a metastable nanocrystalline structure.

Leibniz Gemeinschaft

IFW

Leibniz-Institut
für Festkörper- und
Werkstoffforschung
Dresden

IFW Dresden e. V. · Postfach 27 01 16 · 01171 Dresden

Institut für Komplexe Materialien (IKM)
Direktor: Prof. Dr. Jürgen Eckert

Dr. Norbert Mattern
Abteilungsleiter Strukturforschung

Tel: + 49 (0) 351 4659-367
Fax: + 49 (0) 351 4659-452
E-Mail: n.mattern@ifw-dresden.de

2011-12-16

ACTA MATERIALIA

Dear Professor Hono,

enclosed I send you the revised manuscript

"Structural and Magnetic Nano-clusters in $Cu_{50}Zr_{50-x}Gd_x$ (x = 5 at%) Metallic Glasses"

As proposed by the referee, we removed the surface oxide phase and could repeat SAXS and XRD measurements of the as-quenched and for two annealed states. The SAXS and XRD of the grinded ribbons show the identical results of phase separation (673 K) and crystallization (723 K). Therefore, we are quite sure that the surface oxidation does not influence the phase separation and crystallization of the sample volume.

We also noticed that the surface oxidation of the samples occurs over longer time periods after several months, or now 1,5 years. The almost all results reported in the paper were measured shortly after the preparation of the ribbons (SAXS/WAXS – after 4 weeks, APT after 3 month, ribbons were stored in a glove box). To that time, no oxide film was seen in the XRD (sample surface was shiny, now it is gray). The shown XRD patterns were measured 1 year later, mainly for the phase determination. Unfortunately I did not notice that fact of the surface oxide contributions.

From our investigations we believe, that the phase separation and the surface oxidation are two different issues for the glass under investigation.

The following changes in the revised version:

1. We exchanged the diffraction patterns showing now those of the grinded samples (as-quenched, annealed 400°C, annealed 450°C) in order to be consistent with the SAXS/WAXS data and avoid possible confusions.
2. we deleted the part of the text which was inserted first in order to comment the oxide reflections in diffraction patterns
3. we added at the end of 2. Experimental some sentences in order to mention the occurrence of surface oxidation:" We noticed that colour of the ribbons surface changed over a longer period after several months. We could prove that this surface oxidation

(weak ZrO_2 reflections occur in the XRD patterns) had no influence on the phase separation. The results reported here were measured shortly after the preparation of the ribbons. Furthermore, repetition of SAXS and XRD measurements with grinded ribbons reproduced the results for as-quenched and annealed states."

We hope, you can find our paper now suitable for publication in Acta Materialia.

Thank You very much for your efforts.

Scincerely yours

Norbert Mattern

Leibniz-Institut
für Festkörper- und Werkstoffforschung Dresden e. V.
Vorstand: Prof. Dr. Ludwig Schultz, Dr. h. c. Rolf Pfrengle
Helmholtzstraße 20 · 01069 Dresden · www.ifw-dresden.de
Telefon +49 (0) 351 4659-0, Telefax +49 (0) 351 4659-540
Mitglied der Leibniz Gemeinschaft

Deutsche Bank · Kto.-Nr. 5 353 131 00 · BLZ 870 700 00
SWIFT (BIC): DEUT DE 8C · IBAN: DE 35 8707 0000 0535 3131 00
Dresdner Bank · Kto-Nr. 4 104 407 00 · BLZ 850 800 00
SWIFT (BIC): DRES DE FF 850 · IBAN: DE03 8508 0000 0410 4407 00
Ust –IDNr. DE 140 303 135 · Steuernummer 203-140-04400
VR Dresden Nr. 1369

***Response to Reviewer**

Reply to the referee report:

We thank the referee for his important hints concerning possible influence of oxides on the phase separation.
We carefully checked the occurrence of the oxide reflections. We realized that the sample surface changes over the time of 1.5 years since the samples were prepared. This is indicated by a change of the colour and is related to the occurrence of the weak oxide (ZrO2) reflections in the XRD patterns (Fig3). However, the phase separation of the as-quenched state as well as the changes upon annealing reported in the paper are not influenced by the surface oxidation. We are sure about that, because:

1. we did the SAXS/WAXS and APT measurement in 2010 with rather fresh samples (< 1 month after melt spinning, the XRD from that time does not show the presence of an oxide film.
2. we proved, that the surface oxide film can be removed by grinding (last week)
3. we repeated the SAXS measurement with a sample after grinding in the as-quenched state and annealed state (this week) and we reproduce the SAXS/WAXS measurements shown in the paper.
4. the modification of the surface for longer times (segregation ,oxidation) is also know for binary Cu-Zr glasses if the samples are stored > several month.
5. the XRD-patterns shown in Figure were measured in 06/2011 after about 1 year storage . The measurements to that time were done mainly for the phase determination.

The following changes were done in the revised version:

1. We exchanged the diffraction patterns showing now those of the grinded samples (as-quenched, annealed 400°C, annealed 450°C) in order to be consistent with the SAXS/WAXS data and avoid possible confusions.
2. we deleted the text which was inserted first in order to comment the oxide diffraction
3. we added at the end of the 2. Experimental some sentences in order to mention the occurrence of surface oxidation:" We noticed that colour of the ribbons surface changed over a longer period after several months. We could prove that this surface oxidation (weak ZrO_2 reflections occur in the XRD patterns) had no influence on the phase separation. The results reported here were measured shortly after the preparation of the ribbons. Furthermore, repetition of SAXS and XRD measurements with grinded ribbons reproduced the results for as-quenched and annealed states."

The measurements we did are shown in the following:

1. The reflections/surface oxides were not present at the time, when the samples were prepared (04/2010) as shown in Fig. 1. The samples were stored most of the time in a glove box. Only for cutting samples for measurements the ribbons were taken out (for some hours or days, which is no more exactly known). The SAXS/WAXS measurements were done 02.-06.05/2010.

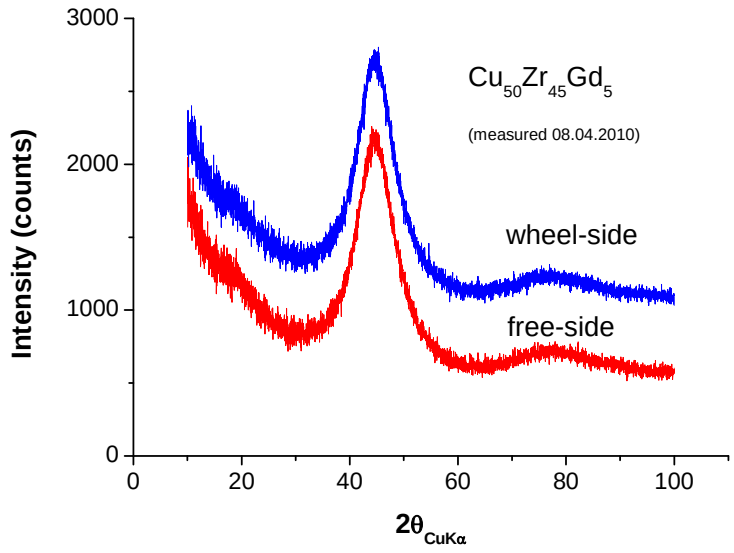

Fig. 1

2. The XRD measurement of the as-quenched sample in 10/2012 (Fig.2). There are no oxide reflection, however the shape of the intensity curve at about 35° shows probably a "beginning" of surface oxide formation

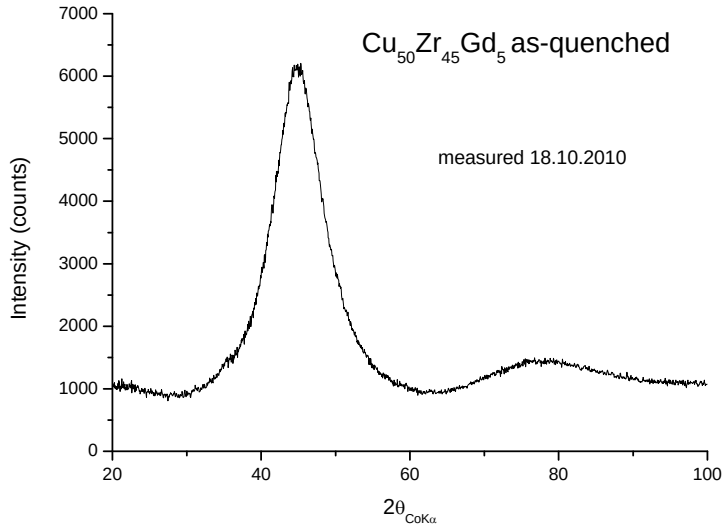

Fig. 2

3. The XRD patterns measured 07.12.2011 shows weak oxide reflections (quite similar like shown in corresponding figure of the submitted paper) , the measurement of the same sample after grinding the surface does not show any contribution of the oxide film (Fig.3).

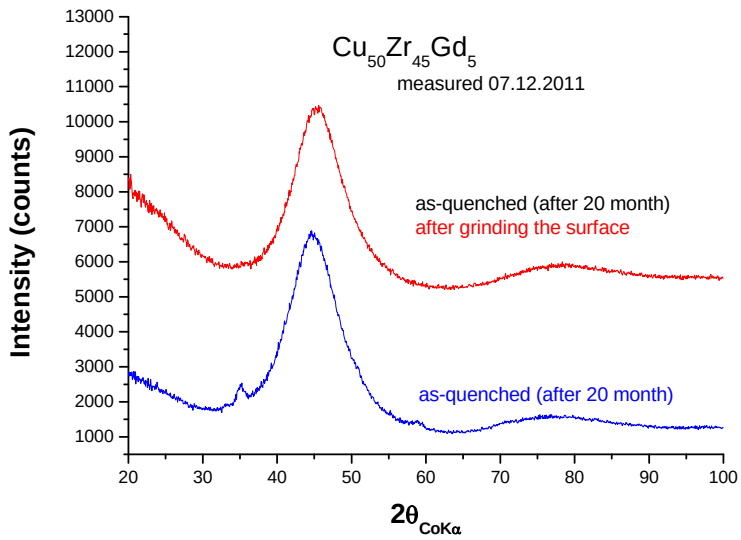

Fig.3

4. The SAXS measurements 14.12.2011 (Fig. 4) of the grinded samples are in a good accordance with the data reported in the paper.

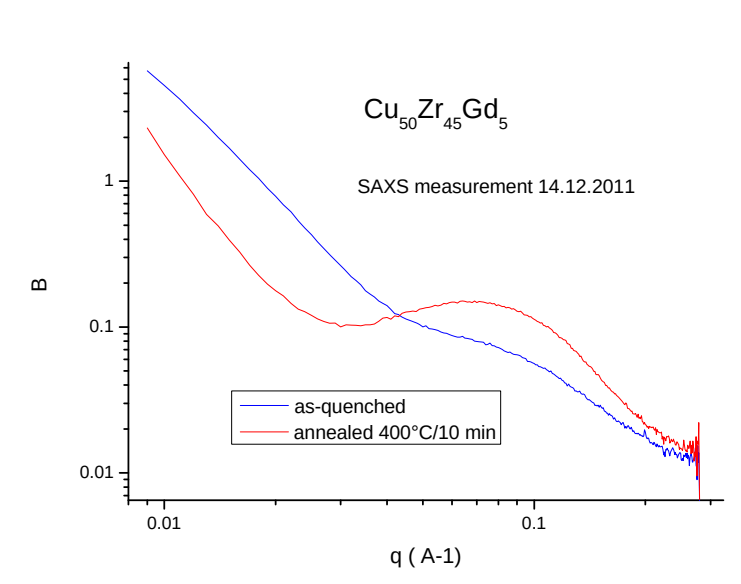

Fig. 4

Structural and Magnetic Nano-clusters in $Cu_{50}Zr_{50-x}Gd_x$ (x= 5 at%) Metallic Glasses

N. Mattern [1,*], A. Shariq[2], B. Schwarz[1], U. Vainio[3], J. Eckert[1,4]

[1]*IFW Dresden, Institute for Complex Materials, Helmholtzstr. 20, 01069 Dresden, Germany*
[2]*FhG Center Nanoelectronic Technology, Koenigsbruecker Strasse 180, D-01099 Dresden, Germany*
[3]*HASYLAB at DESY, Notkestr. 85, 22603 Hamburg, Germany*
[4]*TU Dresden, Institute of Materials Science, Helmholtzstr. 7, 01069 Dresden, Germany*

Abstract

It is shown that phase separated metallic glasses on the nanoscale can be prepared by rapid quenching of $Cu_{50}Zr_{50-x}Gd_x$ melts with low concentration of gadolinium (x = 5 at%). Gd-enriched clusters of 2 nm size are formed as early stages of decomposition in the deeply undercooled melt. The key physical parameter to obtain such nano clustered microstructure upon quenching is the critical temperature of liquid-liquid phase separation which has to be close to the glass transition temperature. Thus, the thermodynamic properties of the liquid phase even in the metastable deeply under-cooled melt determine essentially the structure formation. Analysis of spatial atomic arrangement by atom probe tomography after annealing in the super-cooled liquid state gives direct evidence of the spinodal character of decomposition by up-hill diffusion. The Gd-enriched nano-clusters exhibit ferromagnetic ordering below 50 K and the cluster size regime derived from magnetization measurements is in good agreement with that obtained from atom probe tomography investigations. First stage of crystallization of $Cu_{50}Zr_{45}Gd_5$ glass is observed to be Ostwald type ripening on a nanoscale. The phase separated glass acts as a precursor for the formation of a metastable nanocrystalline structure.

*) corresponding author: n.mattern@ifw-dresden.de

1. Introduction

Metallic glasses can be obtained for several alloy systems by rapid quenching of the melt if the cooling rate is sufficiently high to avoid crystallization. During quenching the liquid becomes strongly undercooled and freezes into a glass at the glass transition temperature T_g. Usually metallic liquids and the corresponding glasses are homogeneous concerning chemical compositions down to the nanometer scale. On the other hand, about 10 % of the published binary alloy systems exhibit a miscibility gap in the equilibrium melt [1] i.e. phase separation into two liquids occurs above the liquidus temperature (critical temperature T_{crit}> liquidus temperature $T_{liquidus}$). There are also examples where a metastable miscibility gap exists in the undercooled metallic liquid (T_{crit}< solidus temperature $T_{solidus}$) like in the binary Co-Cu system [2]. From a thermodynamic point of view these alloy systems are characterized by a positive enthalpy of mixing ($\Delta H_{mix}>0$) between the constituents. In ternary or multi-component systems like e.g. Ni-Nb-Y [3] the miscibility gap in the liquid of a binary subsystem may become extended to a wide field of compositions depending on the thermodynamic properties of the melt.

Recently, metallic alloys showing phase separation in the liquid could be frozen into phase separated metallic glasses by rapid quenching the melt [4-6]. In order to obtain phase separated glass the strategy is to modify alloys with high glass forming ability by adding an element with large positive enthalpy of mixing to at least one other of the constituent. Because binary $Cu_{50}Zr_{50}$ exhibits high glass forming ability (bulk metallic glasses can be prepared by copper-mold casting [7-9]) and Gd has a positive enthalpy of mixing with Zr ($\Delta H_{Gd\text{-}Zr}$= +9 kJ/mol [10]), ternary $Cu_{50}Zr_{50-x}Gd_x$ alloys are suitable candidates to prepare phase separated glasses by rapid quenching the melt. Here, we report on the microstructure formation of ternary metallic glasses with low Gd-content ($x \leq 5$at%). We will show that depending on the composition early stages of phase separation or homogeneous glasses are obtained.

2. Experimental

Pre-alloy were produced from the pure elements by an arc-melter under argon atmosphere. Glassy ribbons 3 mm in width and 30 μm in thickness were prepared by single-roller melt spinning. X-ray diffraction (XRD) with CoK_{α} radiation was done using a X'Pert diffractometer (Panalytical) in Bragg-Brentano geometry. Differential Scanning Calorimetry (DSC) experiments were performed employing a Netzsch DSC 404 calorimeter with a heating rate of 20 K/min. A dual focus ion beam system (FEI Strata 400) was used for the fabrication of the Atom Probe Tomography (APT) tips and Transmission Electron Microscopy (TEM) samples. The APT specimens were analyzed using the local electrode atom probe (LEAP 3000 X Si™) equipped with diode-pumped solid-state laser operating at the second harmonic frequency of 532 nm with a pulse duration of ~ 10 ps and a laser spot size < 10 μm. Pulse laser atom probe analyses were carried out at 27 K and an average detection rate of 0.005 ions/pulse. The TEM was performed using FEI Tecnai F20 XT/STEM operating at 200 kV. Magnetic measurements were conducted using a Quantum Design MPMS-XL-7AC SQUID magnetometer. Small angle X-ray scattering (SAXS) was measured at the B1 synchrotron beam line of HASYLAB/DESY using an energy of 16006 eV. Samples were mounted on a heating stage which was used under vacuum for in-situ measurements. SAXS intensity curves were registered by a PILATUS 300k area detector at a distance covering a *q*-range between 0.2 and 4.3 nm^{-1}. The temperature was stepwise increased. For each temperature background was measured followed by a calibration standard (glassy carbon) and subsequent measurement of the sample. For isothermal analysis the samples were heated with 100 K/min up to the corresponding temperature and measurements were immediately started (5 min or 15 min per pattern) and repeated up to 10 hours. Simultaneously the Wide-angle X-ray Scattering (WAXS) was recorded by a linear position sensitive detector (MYTHEN). We noticed that colour of the ribbons surface changed over a longer period after several months. We could prove that this surface oxidation (weak ZrO_2 reflections occur in the XRD patterns)

had no influence on the phase separation. The results reported here were measured shortly after the preparation of the ribbons. Furthermore, repetition of SAXS and XRD measurements with grinded ribbons reproduced the results for as-quenched and annealed states.

3. Experimental Results

3.1 In situ investigations of the thermal behaviour of $Cu_{50}Zr_{50-x}Gd_x$ metallic glasses

The amorphous structure of the as-quenched ribbons was ascertained by the XRD, TEM and DSC measurements. Figure 1 shows the thermal behaviour of the as-cast $Cu_{50}Zr_{50-x}Gd_x$ glasses by the DSC scans upon continuous heating. The occurrence of the glass transition in a range of about $T_g \approx 670$ K and the exothermic crystallization event at about $T_x \approx 710$ K are evidence for the glassy nature of the ribbons. With Gd addition the crystallization temperature decreases and the crystallization sequence becomes altered. The Gd-containing glasses exhibit a two step crystallization accompanied by two exothermic events in the DSC measurement. The phase sequence and the decomposition behaviour can be concluded by the simultaneous measurements of SAXS and WAXS data given in Figure 2. Figures 2 d-f) show the WAXS patterns of the different $Cu_{50}Zr_{50-x}Gd_x$ glasses at elevated temperatures. The diffuse character of the maxima and the absence of any crystalline reflections indicate the amorphous structure of the as-quenched state, which is preserved up to temperatures T > 700 K. In accordance with the DSC results crystallisation starts depending on the Gd-content between 703 and 723 K. For the binary $Cu_{50}Zr_{50}$ glass the eutectic crystallization is evident by simultaneous formation of the equilibrium phases $Cu_{10}Zr_7$ and $CuZr_2$ at about 723 K (Fig. 2d). The $Cu_{50}Zr_{48}Gd_2$ (Fig. 2e) and $Cu_{50}Zr_{45}Gd_5$ (Fig. 2f) metallic glasses exhibit a changed phase sequence. A mixture of metastable phases is formed as the first stage of crystallization consisting of bcc CuZr and Cu_2Zr-type phase. The strong broadening of the reflections is an

indication of the nanometer crystal size of the metastable phases. At higher temperature between 770 and 820 K, the transformation takes place into the equilibrium phases $CuZr_2$, $Cu_{10}Zr_7$ and Cu_2Gd (not shown here) accompanied by growth of the crystals.

The occurrence of heterogeneities in the as-quenched state and upon heating of the $Cu_{50}Zr_{50-x}Gd_x$ glasses can be seen by the SAXS curves as given in Figures 2 a-c**)**. A very low SAXS intensity is observed for the as-quenched state of $Cu_{50}Zr_{50}$ (Fig. 2a) and $Cu_{46}Zr_{45}Gd_2$ (Fig. 2b) glasses. Therefore, the as-quenched state of these ribbons is homogeneous without any indication of phase separation. The increase of the intensity for q < 0.5nm-1 we observe also for other "homogeneous" metallic glasses which is probably related to surface roughness effects. For the $Cu_{50}Zr_{50}$ glass the SAXS intensities does not change upon heating up to 673 K and only weak increase occurs between 673 and 713 K which may related to the beginning nucleation. With crystallization at T_x= 723 K the SAXS intensity of the $Cu_{50}Zr_{50}$ sample strongly enhances due to the formed heterogeneous two phase mixture. For the $Cu_{46}Zr_{45}Gd_2$ glass the SAXS intensities start to increase gradually at T=633 K. The behaviour between 643 and 713 K indicates nucleation and growth of clusters in the glass well below the crystallization temperature T_x. The monotonic q-dependence of the SAXS intensities points to the formation of uncorrelated, randomly distributed clusters with a certain size distribution. The onset of crystallization at T_x= 723K is reflected by an abrupt change of the shape and the intensity of the SAXS versus temperature.

The SAXS patterns of the $Cu_{50}Zr_{45}Gd_5$ metallic glass shown in Figure 2 c) behave completely different. A weak correlation maximum at q_{max} =1.2 nm^{-1} is observed in the SAXS curve of the as-quenched state. Such an interference maximum indicates the presence of compositional fluctuations with a dominant correlation length. Using the relationship $\zeta = 2\pi/q_{max}$ between the correlation length ζ and the position of the maximum q_{max} one obtains a value of ζ = 5 nm. Almost identical SAXS curves are obtained upon heating up to T= 603 K. From T= 603 K the intensity of the maximum increases obviously but the position q_{max}

becomes only slightly shifted. Such behaviour is typical for early stages of spinodal decomposition where first the amplitudes of the chemical fluctuations increase [11,12]. With further increasing temperature up to T= 693 K we observe an on-going phase separation prior to crystallization, which starts at T_x= 703 K for the step-wise heating. Again, with the onset of the crystallization an abrupt change occurs of the shape and the intensity of the SAXS curves.

3.2 Microstructure of as-quenched and annealed of $Cu_{50}Zr_{50-x}Gd_x$ metallic glasses

Figure 3 shows the room temperature XRD patterns of different pieces of the $Cu_{50}Zr_{45}Gd_5$ glassy ribbons in the as-quenched state and after heat treatments at different temperature T_A each for 10 min. The glassy state of the as-quenched state and after annealing at T_A= 673 K is demonstrated by the diffuse character of XRD pattern. In accordance with the crystallization temperature derived from the DSC curve, the sample annealed at T_A =723 K is crystallized. The Gd addition leads to the formation of metastable phases CuZr + Cu_2(Gd,Zr) as the first stage of crystallization. The broadening of the reflections indicates that the crystallites are only some nanometers in size. After annealing at higher temperature T_A = 873 K, corresponding to the second exothermic DSC event, the metastable phases are transformed into the equilibrium state consisting of $CuZr_2$, $Cu_{10}Zr_7$ and Cu_2Gd which is accompanied by crystal growth as can be seen by sharpening of the reflections in Fig.3.

Figure 4a) shows the TEM image of $Cu_{50}Zr_{45}Gd_5$ glass after annealing in the supercooled liquid state (T_A=673 K //10min). The homogeneous contrast without any indication for the presence of crystallites gives evidence for the glassy structure which is still preserved after the heat treatment in the supercooled liquid ($T_g < T_A < T_x$). The TEM image does not give any indication of a heterogeneous microstructure, however this is due to limitations concerning the spatial resolution of TEM with respect to the small size and the continuous profile of the concentration fluctuations. The TEM image of the annealed glass at

T_A=723 K (Figure 4b) clearly shows the presence of nanocrystals of about 5 nm in size in accordance with XRD results.

The ATP results of the as-quenched and annealed samples are compared in Figures 5-7. Figure 5 a-c) show the spatial distributions of the constituent elements of the $Cu_{50}Zr_{45}Gd_5$ glasses for the as-quenched state as well as after annealing below and above the first crystallization event. Iso-concentration surfaces are depicted in order to elaborate the interface regions of the Gd-enriched clusters. The used values of Gd iso-concentration are to certain extend arbitrary because the concentration varies continuously between clusters and matrix. The visible cluster size therefore depends on the chosen value however the clustered structure behind is well demonstrated (the spatial distribution of only the Gd atoms are given in the graphical abstract). For the as-quenched ribbon the 3D-AP micrograph clearly illustrates a heterogeneous microstructure with Gd-enriched clusters randomly distributed throughout the analysed volume with diameters in a range from 2 -3 nm. Annealing of the $Cu_{50}Zr_{45}Gd_5$ metallic glass changes the element concentration distribution as can be seen by the spatial atomic arrangements of Figures 5 b-c). In contrast, there is no obvious heterogeneity in the as quenched $Cu_{50}Zr_{48}Gd_2$ metallic glass shown in Figure 5 d) which is in accordance with the SAXS measurements. Figures 6 a - d present the corresponding concentration profiles along a cylinder of 2 nm diameter through the analysed volumes of Figures 5 a-d). The concentration profiles indicate clearly the fluctuation of the gadolinium content. Gd enrichment is accompanied by a simultaneous enrichment of Cu and depletion of Zr compared to the nominal composition of the alloy. The concentration depth profile in Figure 6 b) illustrates that annealing the metallic glass in the supercooled liquid state results in a further accumulation of Gd and Cu and a corresponding depletion of Zr within the phase separated regions and gives a direct evidence of an up-hill diffusion pointing to the spinodal character of the phase separation. Annealing at T_A= 723 K led to crystallization as proven by TEM and XRD and growth of the Gd rich phase up to 5 nm which is also visible by the extension of the

concentration fluctuations in Fig. 6 c). The corresponding ATP image Fig. 5c) shows that crystallization and growth are accompanied by coalescence of neighboured clusters.

In order to characterize the microstructure of the whole volume analysed, the proximity method [13] was used. By this method the average alloy composition is calculated in predefined thin shells as a function of the distance from a selected surface irrespective of its convexity. The proximity histograms for the as-quenched and the annealed $Cu_{50}Zr_{45}Gd_5$ glasses are shown in Figure 7. The curves represent for each sample the average of spatial concentration distribution of at least 200 clusters and their surroundings. The values of cluster composition, size and density as well as the composition of the surrounding matrix were calculated from the proxigrams and are summarized in Table 1. Phase separation results in Gd-enriched clusters for as quenched $Cu_{50}Zr_{45}Gd_5$ glass having local chemical composition of $Cu_{52}Zr_{34}Gd_{14}$. The interface between cluster and surrounding matrix exhibits a continuous element distribution. Taking the full width at half of the maximum value of the Gd-concentration within a cluster as a measure of cluster size, a mean size of 2.8 nm can be estimated for the as-quenched state. The sample annealed at T_A= 673 K is characterized by an increased content of Gd and Cu in the clusters at the expense of Zr. The resultant composition of about $Cu_{59}Zr_{25}Gd_{16}$ is revealed from the proximity histogram. The average cluster size only slightly increased whereas the number density stays almost constant (Table 1). From a comparison of the concentration profiles for different heat treatments, an up-hill diffusion of Gd and Cu from the surrounding into the clusters can unambiguously be concluded. By annealing in the supercooled liquid state the amplitude of the fluctuations increases in accordance with the SAXS observations, which gives evidence of a spinodal mechanism clearly distinguished from concentration profiles for nucleation and growth [12].

With crystallization, the size of the cluster increases and consequently the number density becomes reduced (Table 1). The microstructure (Fig. 5c) indicates that the crystallization is accompanied by Ostwald-type mechanism of growth. The analysis of the

local composition of the formed nanocrystallites gives $Cu_{60}Zr_{17}Gd_{23}$ for the metastable phase which is surrounded by the likewise metastable $Cu_{49}Zr_{48}Gd_3$ matrix phase (Table 1).

3.3 Magnetic properties of $Cu_{50}Zr_{50-x}Gd_x$ metallic glasses

Binary $Cu_{50}Zr_{50}$ glass only exhibits temperature independent weak Pauli paramagnetism for T > 2 K. Therefore, the measured total magnetic moment of the the ternary $Cu_{50}Zr_{50-x}Gd_x$ glasses can be assumed to originate exclusively from the localized Gd *f* electron magnetic moments to a good approximation. Nevertheless, the conduction band of the Cu-Zr host metal plays a crucial role concerning the indirect exchange interactions among Gd atoms [14,15]. Figure 8 shows the inverse dc susceptibility versus temperature of $Cu_{50}Zr_{50-x}Gd_x$ glasses. Except for $Cu_{50}Zr_{45}Gd_5$ glassy sample that was crystallized after annealing at 723 K, all samples show a linear dependence down to the temperature $T_{p,min}$ (see Table 2). In this temperature region the Weiss constant θ and the Curie constant *C*, respectively the effective paramagnetic moment μ_{eff}, can be obtained from a fit to the Curie-Weiss law:

$$\chi = C/(T-\theta) \qquad (1).$$

For $Cu_{50}Zr_{48}Gd_2$ the effective moment μ_{eff} = 7.83(1) μ_B per Gd atom is close to that of the theoretical magnetic moment of Gd_{3+} with S=3.5 (7.9 μ_B) and θ = 7.0(1) K shows that only very weak mean-field ferromagnetic coupling is present. For $Cu_{50}Zr_{45}Gd_5$ glass the effective magnetic moment is increased to a value μ_{eff} ~ 8.5 μ_B per Gd atom due to the heterogeneous distribution of the Gd atoms. Also the Weiss constant that increased to about 20 K gives evidence for a stronger mean field ferromagnetic coupling.

The magnetic ordering of the $Cu_{50}Zr_{45}Gd_5$ glass was analyzed by temperature dependent magnetization versus field measurements $M(H)_T$ in the range 5 K ≤ T ≤ 50 K . Figure 9 shows the corresponding curves for the as-quenched state. The experimental data can not be described well by a single Brillouin function which is the quantum-mechanical solution of the field dependence of a given non-interacting spin system. Taking into account the presence of

two types of Gd environments, i.e. rather isolated Gd atoms distributed within the matrix and those in the Gd-enriched clusters as observed by APT, one has to assume two types of spin quantum numbers or the superposition of two Brillouin functions $B_i(\zeta)$ (i=1,2). The experimental curves in the temperature range 5 K ≤ T ≤ 50K then can be described by:

$$M(H,T)= \sum \boldsymbol{N}_i * \boldsymbol{m}_i * B_i(\zeta) \ , \quad \zeta=(\boldsymbol{m}_i / k_B T)*H \ . \qquad (2)$$

The one part of the sum (i=1) describes the magnetic contribution of the Gd-enriched clusters and the other (i=2) that of the Gd-atoms of the surrounding "matrix" phase. The magnetic moments $\boldsymbol{m}_i^*$ and the number $\boldsymbol{N}_i$ of the Gd-clusters can be estimated by fitting equ. (2) to the measured data. The comparison of the resulting fit-curves with the experimental data is also given in Figure 9. As can be seen, a good agreement is obtained by the simple mixture model in a temperature range 10 K ≤ T ≤ 50 K. The calculated values $\boldsymbol{m}_i^*$ and $\boldsymbol{N}_i$ are summarized in Table 3. Assuming that the magnetic moment of the Gd atoms is 7.9 μ_B, corresponding to a Gd^{3+} with S = 3.5, one can estimate the number of atoms contributing to the magnetic moment of one cluster with $\boldsymbol{m}_i^*$. From the data obtained it follows that in the as-quenched $Cu_{50}Zr_{45}Gd_5$ glass for T < 25 K magnetic clusters are formed by about 20 Gd atoms. Only a certain part of about 15-20 % of all Gd-atoms contribute to these larger magnetic clusters, whereas the rest is distributed within the matrix phase without or only weak magnetic interaction with Gd neighbours. The temperature dependent magnetization versus field curves of the as-quenched $Cu_{50}Zr_{48}Gd_2$ glass and the annealed state of $Cu_{50}Zr_{45}Gd_5$ glass are qualitatively similar to those shown in Figure 9. The corresponding data of magnetic cluster size and density are given in Table 3. For the as-quenched state of $Cu_{50}Zr_{48}Gd_2$ glass the Gd-rich clusters consist of about 5 Gd-atoms only. For the 400°C annealed $Cu_{50}Zr_{45}Gd_5$ sample the number of Gd-atoms in the cluster increases to about 40, however the number of clusters remains nearly constant. For T= 5K clear deviation between measured and calculated data are visible in Figure 9. Due to the occurrence of coupling between the ferromagnetic clusters at T< 10K, the preposition of non interacting magnetic clusters is no more valid.

Using the compositions of the Gd-enriched clusters as determined by APT one can estimate the size of the magnetic clusters. For the as-quenched $Cu_{50}Zr_{45}Gd_5$ glass the magnetic cluster consists of about 150 atoms, and for the at 673 K annealed state of 300 atoms respectively. With an atomic density of ρ_0 = 60 nm^{-3} the diameter of the magnetic clusters are 1.4 nm, and 1.7 nm respectively which is in a good accordance with the cluster size from the APT results.

For $Cu_{50}Zr_{48}Gd_2$ and $Cu_{50}Zr_{45}Gd_5$ glasses the zero-field-cooled (ZFC) and field-cooled (FC) magnetization are shown in Figure 10, measured with increasing temperature from 2 K up to 350 K at a field of 100 Oe. The ac-susceptibility's real part Re(χ) for an excitation with 3.9 Oe at ω = 1, 10, 100 and 1000 Hz, respectively, in zero dc-field is given for all samples. The temperature T_f, at the maximum in the ac-susceptibility's real part at 1 Hz, and its frequency shift $S_F = \Delta T_f/[T_f \Delta(\log \omega)]$ with varying frequency are presented in Table 2. $Cu_{50}Zr_{48}Gd_2$ as prepared (a) shows monotonically increasing ac-susceptibility down to 2 K with all frequency curves superimposing and there is negligible bifurcation between the ZFC and FC magnetization branch. All results together essentially prove paramagnetic behaviour down to lowest temperature with an effective moment μ_{eff} = 7.83(1) μ_B. In contrast, glassy $Cu_{50}Zr_{45}Gd_5$ as prepared (b) exhibits a maximum in the ac-susceptibility at T_f = 2.8(2) K for ω = 1 Hz that is shifted to higher temperatures with S_F = 0.033(2). In the same temperature region the ZFC and FC magnetization starts to bifurcate indicating irreversible processes of magnetization. The peculiar difference of the ZFC and FC magnetization branch below T_f, but especially the frequency shift of 0.03 is typical for spin glass, respectively cluster glass behaviour [14]. According to [15] the rounded susceptibility maxima observed at the ‚freezing' temperatures allows for the classification as cluster glass. Still paramagnetic contributions are suggested for $Cu_{50}Zr_{45}Gd_5$ annealed at T_A= 673 K (c) the maximum of the ac-susceptibility's real part has considerably shifted to T_f = 5.4(2) K for ω = 1 Hz and S_F increases to 0.062(1). At 2 K the ac-susceptibility for all frequencies has again decreased

despite the existence of weak ferromagnetic interactions. The ac-susceptibility with frequency dependent shift of the maximum as well as the typical progression of ZFC/FC magnetization measurements clearly indicate, that the major part of the sample behaves cluster glass-like. The rate of frequency shift is S_F = 0.062(1) and is therefore still in the range typical for cluster-glasses. The crystallization after annealing the $Cu_{50}Zr_{45}Gd_5$ glass at T_A= 723 K remarkably modifies the magnetic characteristics (d). The ac-susceptibility no longer exhibits a maximum, but increases monotonically with decreasing temperature. A weak frequency dependence is visible. There is still a bifurcation of the ZFC and FC branch, but the FC magnetization is still increasing considerably below the bifurcation temperature and the ZFC magnetization does not approach zero magnetization.

The features of the magnetic hysteresis loops measured at 2 K for the various samples are in agreement with the results of the ZFC/FC measurements in this temperature region. $Cu_{50}Zr_{48}Gd_2$ as-quenched is paramagnetic down to lowest temperatures with superimposing ZFC and FC branch and consequently there is a linear dependence of magnetization on field without any hysteresis Figure 11a). The pronounced bifurcation between the ZFC and FC branch below 6 K found for $Cu_{50}Zr_{45}Gd_5$ annealed at 673 K is also reflected by a pronounced hysteresis in the magnetization versus field measurement (Figure 11 c). $Cu_{50}Zr_{45}Gd_5$ annealed at 723 K has already crystallized and shows a less pronounced bifurcation between the ZFC and FC. Accordingly also the hysteretic features are less pronounced (Figure 11 d) again.

4. Discussion

The structure formation can be understood by the Cu-Zr-Gd phase diagram. Figure 12 shows a pseudo-binary section $Cu_{50}Zr_{50}$-$Cu_{50}Gd_{50}$ of the ternary Cu-Gd-Zr phase diagram calculated by the CALPHAD method [16]. The assessment was done by an extrapolation of the corresponding binary phase diagrams [17-19] using the sub-regular solution model. The metastable miscibility gap originating from the binary Gd-Zr system becomes extended into

the ternary Cu-Gd-Zr as indicated by the binodal curve. Also depicted are the values of the glass transition temperatures of $Cu_{50}Zr_{50-x}Gd_x$ (x= 0, 2, 5) glasses as determined by the DSC scans. The critical temperature of liquid-liquid decomposition T_{crit} depends strongly on the chemical composition. For the $Cu_{50}Zr_{48}Gd_2$ glass an almost homogeneous glassy state is obtained because T_{crit} is lower than the glass transition temperature T_g. The $Cu_{50}Zr_{45}Gd_5$ glass is characterized by early stages of spinodal decomposition in the as-quenched state because T_{crit} is above T_g however the difference is small. Annealing the glass leads to further development of the decomposition as shown by the in situ SAXS and WAXS data in Figure 2.

The structure formation by spinodal decomposition is usually described by the Cahn-Hilliard-Cook theory [11,12]. The decomposition is initiated via the spontaneous formation and subsequent growth of coherent composition fluctuations. Figure 13 a) shows a model function for a spatial concentration fluctuation $c(r)$=A* cos(1.26*r) representing a constant fluctuation length of 5 nm. The Fourier form gives the corresponding SAXS intensities as presented in Figure 13 b). The corresponding $I(q)$ curves describe qualitatively the experimental findings shown in Figure 2 c) upon heating within the glassy and the supercooled liquid state. Figure 14 shows the measured in situ SAXS patterns of the $Cu_{50}Zr_{45}Gd_5$ glass under isothermal conditions at T=633 K and T=648 K as a function of time. With increasing time, the height or integral intensity of the maximum enlarges. The maximum position q_{max} = 1.2 nm^{-1} remains nearly unchanged during the heat treatment. Therefore, the behaviour of the SAXS intensities during isothermal annealing corresponds to a spinodal mechanism. Simultaneous measured XRD patterns (not shown here) give evidence that phase separation takes place within the glassy state. As expected for a thermal activated process, at the higher temperature the decomposition develops faster.

5. Conclusion

Phase separated metallic glasses can be prepared in the Cu-Zr-Gd system by rapid quenching of the melt. The structure formation as a function of the Gd content is essentially determined by the composition dependence of the miscibility gap of the metastable undercooled melt. Early stages of spinodal decomposition or almost homogeneous glassy states are obtained if the critical temperature of liquid-liquid phase separation is close or below to the glass transition temperature. Direct evidence of the phase separation was obtained by atom probe tomography showing Gd-enriched clusters of 2- 5 nm size for the $Cu_{50}Zr_{45}Gd_5$ glass. On-going phase separation of the glasses prior to crystallisation could be observed by simultaneous measurements of SAXS and WAXS at elevated temperature. Magnetic ordering at low temperature occurs in the $Cu_{50}Zr_{45}Gd_5$ glass as a consequence of the phase separation and the formation of Gd-enriched nano-clusters.

References

[1] Massalski TB, Subramanian PR, Okamoto H, L. Kacprzak L. (ed.) "Binary Alloy Phase Diagrams", ASM International Materials Park, OH, 1990.

[2] Cao CD, Görler GP, Herlach DM, Wei B. Mater Sci Eng 2002; 325: 503.

[3] Mattern N, Zinkevich M, Löser W, Behr G, Acker J. J. Phase Equil.& Diff. 2008;29:141.

[4] Kündig AA, Ohnuma M, Ping DH, Ohkubo T, Hono K. Acta Mater 2004;52:2441.

[5] Park BJ, Chang HJ, Kim DH, Kim WT, Appl Phys Lett 2004; 85:6353.

[6] Mattern N, Kühn U, Gebert A, Gemming T, Zinkevich M, Wendrock H, Schultz L. Scripta Mater 2005;53:271.

[7] Xu D, Lohwongwatana B, Duan G, Johnson WL, Garland G. Acta Mater 2004;52:2621.

[8] Wang D, Li Y, Sun BB, Sui ML, Lu K, Ma E. Appl Phys Lett 2004;84 4029.

[9] Inoue A, Zhang W. Mater Trans 2004;45:584.

[10] Boer FR, Boom R, Mattens WCM, Miedema AR, Niessen AK. "Cohesion and Structure", Vol.1, Cohesion in Metals, Elsevier Science Publishers 1988.

[11] Cahn JW, Hillard JE. J Chem Phys 1959; 31:539. J Chem Phys 1959; 31:688.

[12] Binder K, Fratzl P. "*Spinodal Decomposition" in "Phase Transformations in Material*" ed. G. Kostorz, Wiley-VHC Weinheim 2001

[13] Hellman OC, Vandenbroucke JA, Rusing J, Isheim D, Seidman DN. Mater Res Soc Symp Proc 2000;578:395.

[14] Mydosh JA. "*Spin Glasses: An Experimental Introduction"*; Taylor and Francis: London 1993.

[15] Ododo JC, Coles BR. J Phys F: Met Phys 1977;7:2393.

[16] Saunders N, Miodownik AP. " CALPHAD Calculation of Phase Diagrams"; Pergamon Materials Series 1998.

[17] Zen KJ, Hamalainen M, Lukas HL. J Phase Equil 1994;15:577.

[18] Voskov AL, Uspenskaya IA. Russian J Phys Chem A 2009; 83:604.

[19] Zinkevitch M, Mattern N, Seifert HJ, J Phase Equilibria 2001;22:43.

Acknowledgements

The authors thank B. Arnold and Mr. M Mildner for TEM analysis. Financial support of the Deutsche Forschungsgemeinschaft DFG (Ma1531/10) is gratefully acknowledged.

Figure captions:

Fig. 1: DSC scans of $Cu_{50}Zr_{50-x}Gd_x$ glasses at heating rate 20K/min, a): x=0, b): x=2, and c): x= 5. Glass transition by the endothermic event and crystallization by exothermic events confirm the glassy structure of the rapidly quenched $Cu_{50}Zr_{50-x}Gd_x$ alloys.

Figure 2: In situ SAXS (a-c) and WAXS (d-f) of $Cu_{50}Zr_{50-x}Gd_x$ glasses at room temperature and elevated temperatures upon stepwise heating from 573 K each 10 K up to 773 K (a), d) : $Cu_{50}Zr_{50}$ glass; b), e) : $Cu_{50}Zr_{48}Gd_2$ glass, c), f) $Cu_{50}Zr_{45}Gd_5$ glass). For the $Cu_{50}Zr_{45}Gd_5$ glass, simultaneously measured SAXS (f) and WAXS (c) gives evidence that glass phase separation occurs in the glassy as well as in the supercooled liquid state prior to crystallization.

Figure 3 : Room temperature XRD pattern of $Cu_{50}Zr_{45}Gd_5$ glass, as-quenched state and pieces each annealed at a different temperature for 10 min.

Figure 4: TEM image of $Cu_{50}Zr_{45}Gd_5$ glass a) - after annealing at T_A=673 K // 10 min

(no heterogeneities are visible) b) - after annealing at T_A=723 K // 10 min

(nanocrystallization occured from the heterogeneous glass).

Figure 5: Spatial distribution of the constituent elements as analyzed by atom-probe tomography. a) $Cu_{50}Zr_{45}Gd_5$: as-quenched state b) $Cu_{50}Zr_{45}Gd_5$: after annealing 673 K for 10 min (within super-cooled liquid state) c) $Cu_{50}Zr_{45}Gd_5$: after annealing 723 K for 10 min (above the crystallization temperature) d) $Cu_{50}Zr_{48}Gd_2$: as-quenched state. Iso-concentration surfaces are drawn in green to elaborate the Gd-enriched clusters (7, 11, and 14 at% Gd for a) b), and c) repectively). For clarity, 30% of the atoms Cu (orange), Zr (blue), Gd(green) are shown. A heterogeneous element distribution and Gd-enriched clusters are seen for the $Cu_{50}Zr_{45}Gd_5$ glass. Changes of the microstructure with annealing treatments are evident. For the $Cu_{50}Zr_{48}Gd_2$ glass a homogeneous element distribution is obtained (d).

Figure 6: Composition profile along a selected cylinder of Figure 3 (2 nm in diameter). a) $Cu_{50}Zr_{45}Gd_5$: as-quenched state b) $Cu_{50}Zr_{45}Gd_5$: after annealing 673 K for 10 min (within super-cooled liquid state) c) $Cu_{50}Zr_{45}Gd_5$: after annealing 723 K for 10 min (above the crystallization temperature) d) $Cu_{50}Zr_{48}Gd_2$: as-quenched state. Fluctuations of the chemical composition with nanometer size are visible. Clusters are enriched in Gd and Cu. With annealing treatment the amplitude of the concentration fluctuations increases.

Figure 7: Proximity histograms for as-quenched and annealed $Cu_{50}Zr_{45}Gd_5$ glasses. A statistical average of the element compositions within the Gd-enriched clusters and their surrounding is presented from the analysis of more then 200 clusters. An up-hill diffusion of Gd and Cu atoms is seen by the comparison of the as-quenched state with the 673 K annealed glass. The increase is accompanied by depletion of the elements from the surrounding of the cluster. Both give direct evidence of the spinodal character of the decomposition.

Figure 8: Inverse susceptibility versus temperature of a) $Cu_{50}Zr_{48}Gd_2$: as-quenched state, b) $Cu_{50}Zr_{45}Gd_5$: as-quenched state, c) $Cu_{50}Zr_{45}Gd_5$: after annealing 673 K for 10 min (within super-cooled liquid state), d) $Cu_{50}Zr_{45}Gd_5$: after annealing 723 K for 10 min (above the crystallization temperature). At low temperature the deviation from the linear dependence indicates the transformation from the paramagnetic state to ferromagnetism due to magnetic ordering within the Gd-enriched clusters.

Figure 9: Magnetization versus applied field at low temperatures of as-quenched $Cu_{50}Zr_{45}Gd_5$ glass. The experimental data were fitted by a sum of two Brillion functions (solid lines) representing the magnetic contributions of the Gd atoms in the clusters, and those of the matrix respectively.

Figure 10 : Zero-field-cooled (ZFC) and Field-cooled (FC) magnetization measurements (left side) and ac-susceptibility's real part Re(χ) (right side) in the temperature range from 2 to 10 K for a) $Cu_{50}Zr_{48}Gd_2$: as-quenched state, b) $Cu_{50}Zr_{45}Gd_5$: asquenched state, c) $Cu_{50}Zr_{45}Gd_5$: after annealing 673 K for 10 min (within super-cooled liquid state), d) $Cu_{50}Zr_{45}Gd_5$: after annealing 723 K for 10 min (above the crystallization temperature).

Figure 11: Magnetic Hysteresis Loops at 2 K for a) $Cu_{50}Zr_{48}Gd_2$: as-quenched state, b) $Cu_{50}Zr_{45}Gd_5$: as quenched state, c) $Cu_{50}Zr_{45}Gd_5$: after annealing 673 K for 10 min (within super-cooled liquid state), d) $Cu_{50}Zr_{45}Gd_5$: after annealing 723 K for 10 min (above the crystallization temperature).

Figure 12: Pseudo-binary section $Cu_{50}Zr_{50}$-$Cu_{50}Gd_{50}$ of the Cu-Zr-Gd phase diagram. The temperature of liquid-liquid phase separation depends strongly on the composition as depicted by the bimodal curve.Different microstructures are obtained for rapidly quenched glasses as a consequence of the thermodynamic properties of the undercooled melts with respect to the glass transition temperature, $Cu_{50}Zr_{45}Gd_5$: $T_{crit} \approx T_g$, $Cu_{50}Zr_{48}Gd_2$: $T_{crit} < T_g$.

Figure 13: Schematic presentation of fluctuation in real space and corresponding diffraction in reciprocal space by a spinodal decomposition mechanism [16]: a) Concentration fluctuation $c(r)$ and b) corresponding SAXS intensity $I(q)$ as function of amplitude A.

Figure 14: In situ SAXS measurement of $Cu_{50}Zr_{45}Gd_5$ glass at elevated temperatures, a) T= 623 K, b) T =648 K , Interference maximum at q=1.2 nm^{-1} increases in height with time in accordance with spinodal mechanism.

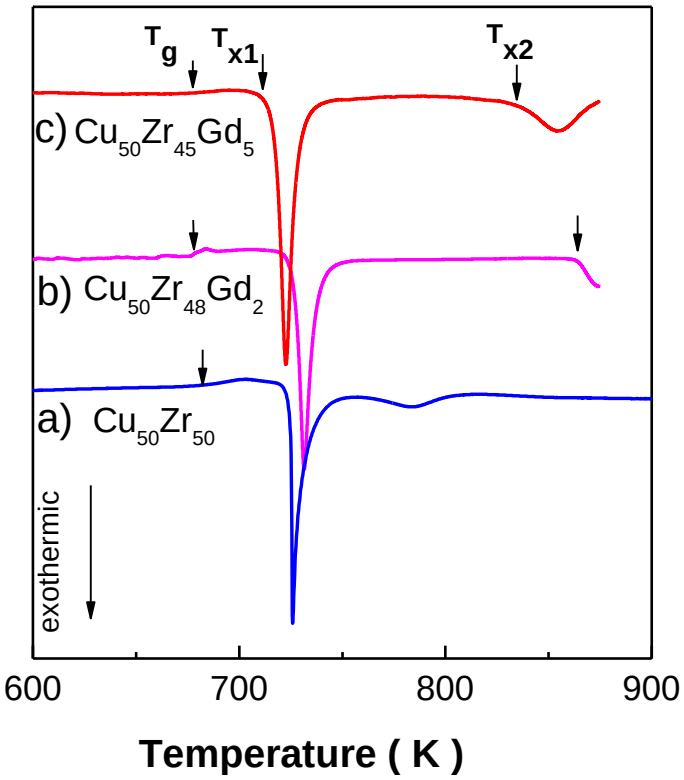

Fig. 1: DSC scans of $Cu_{50}Zr_{50-x}Gd_x$ glasses at heating rate 20K/min, a): x=0, b): x=2, and c): x= 5. Glass transition by the endothermic event and crystallization by exothermic events confirm the glassy structure of the rapidly quenched $Cu_{50}Zr_{50-x}Gd_x$ alloys.

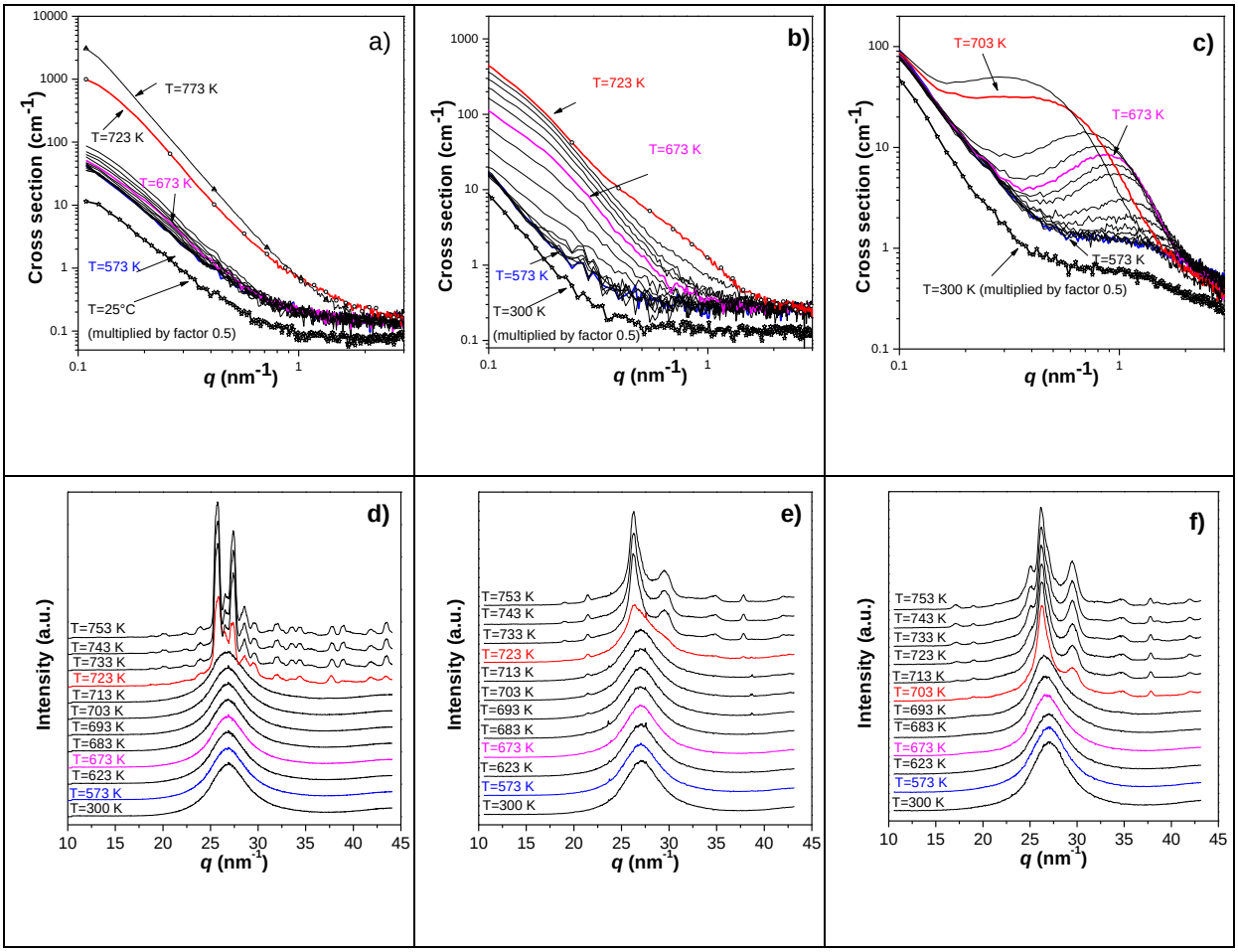

Figure 2: In situ SAXS (a-c) and WAXS (d-f) of $Cu_{50}Zr_{50-x}Gd_x$ glasses at room temperature and elevated temperatures upon stepwise heating from 573 K each 10 K up to 773 K (a), d) : $Cu_{50}Zr_{50}$ glass; b), e) : $Cu_{50}Zr_{48}Gd_2$ glass, c), f) $Cu_{50}Zr_{45}Gd_5$ glass). For the $Cu_{50}Zr_{45}Gd_5$ glass, simultaneously measured SAXS (f) and WAXS (c) gives evidence that glass phase separation occurs in the glassy as well as in the supercooled liquid state prior to crystallization.

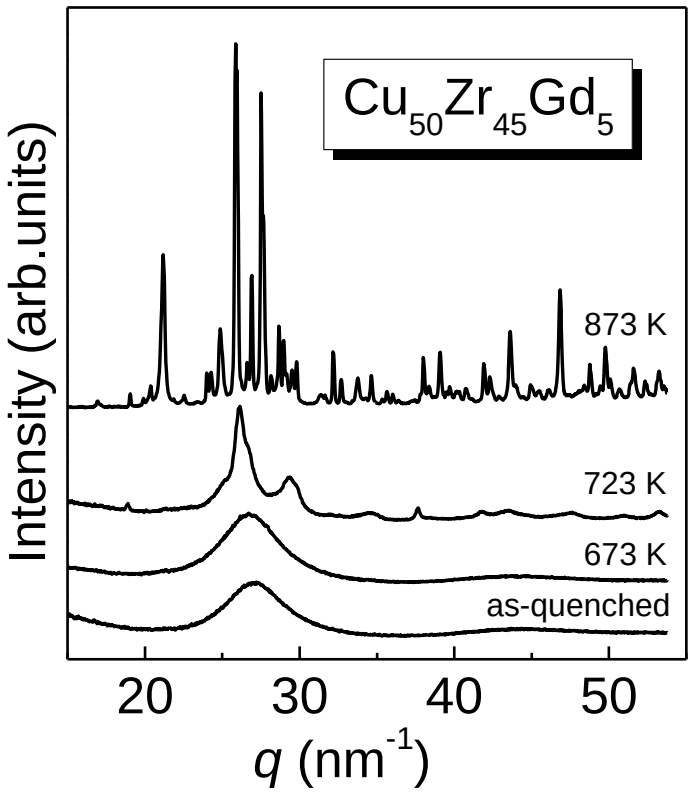

Figure 3: Room temperature XRD pattern of $Cu_{50}Zr_{45}Gd_5$ glass, as-quenched state and pieces each annealed at a different temperature for 10 min.

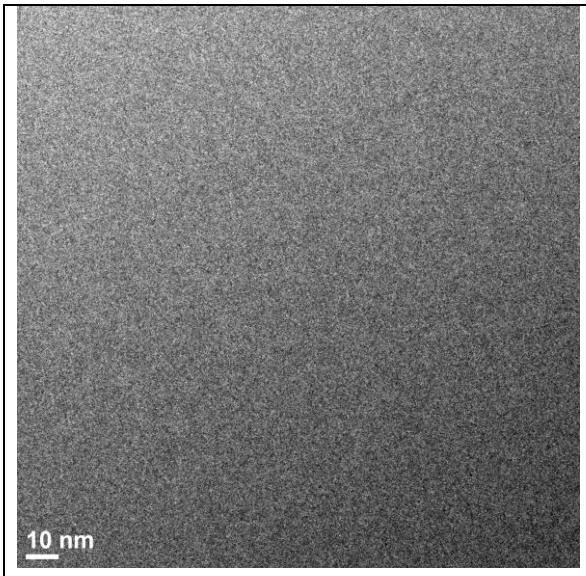

a)

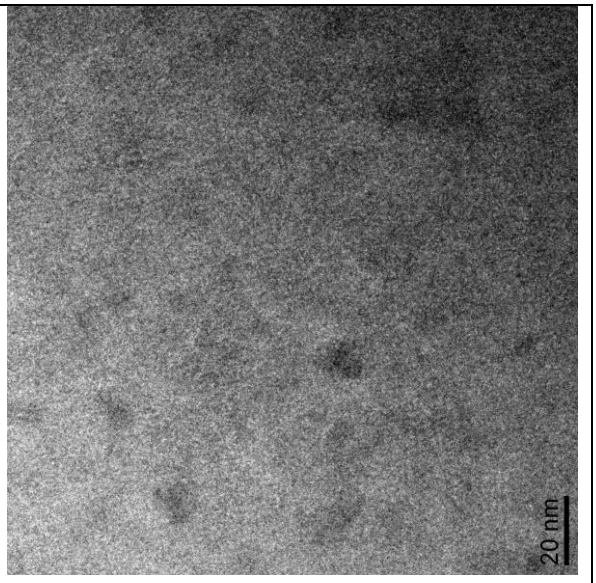

b)

Figure 4: TEM image of $Cu_{50}Zr_{45}Gd_5$ glass a) - after annealing at T_A=673 K // 10 min (no heterogeneities are visible) b) - after annealing at T_A=723 K // 10 min (nanocrystallization occured from the heterogeneous glass).

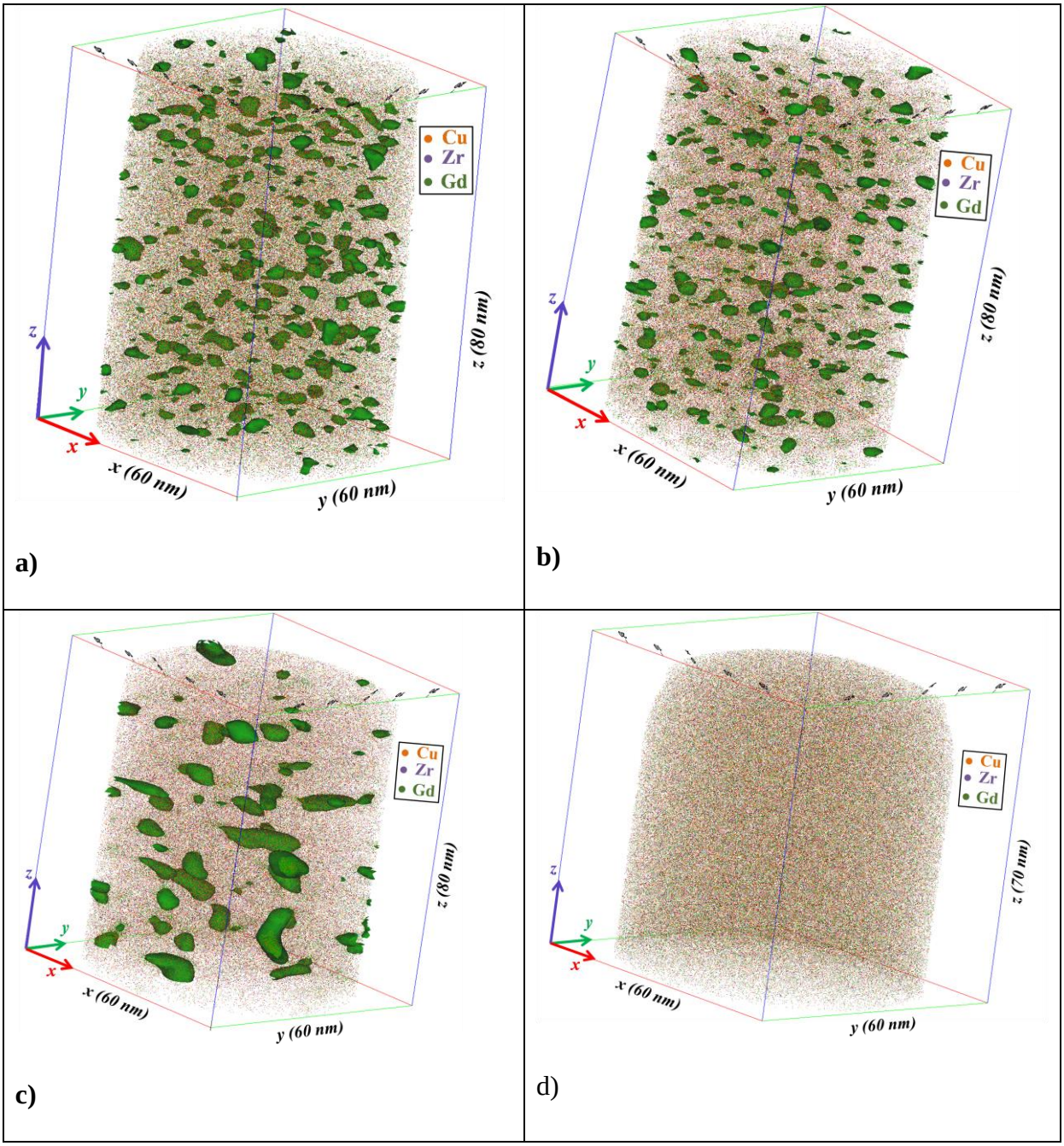

Figure 5: Spatial distribution of the constituent elements as analyzed by atom-probe tomography. a) $Cu_{50}Zr_{45}Gd_5$: as-quenched state b) $Cu_{50}Zr_{45}Gd_5$: after annealing 673 K for 10 min (within super-cooled liquid state) c) $Cu_{50}Zr_{45}Gd_5$: after annealing 723 K for 10 min (above the crystallization temperature) d) $Cu_{50}Zr_{48}Gd_2$: as-quenched state. Iso-concentration surfaces are drawn in green to elaborate the Gd-enriched clusters (7, 11, and 14 at% Gd for a) b), and c) repectively). For clarity, 30% of the atoms Cu (orange), Zr (blue), Gd(green) are shown. A heterogeneous element distribution and Gd-enriched clusters are seen for the $Cu_{50}Zr_{45}Gd_5$ glass. Changes of the microstructure with annealing treatments are evident. For the $Cu_{50}Zr_{48}Gd_2$ glass a homogeneous element distribution is obtained.

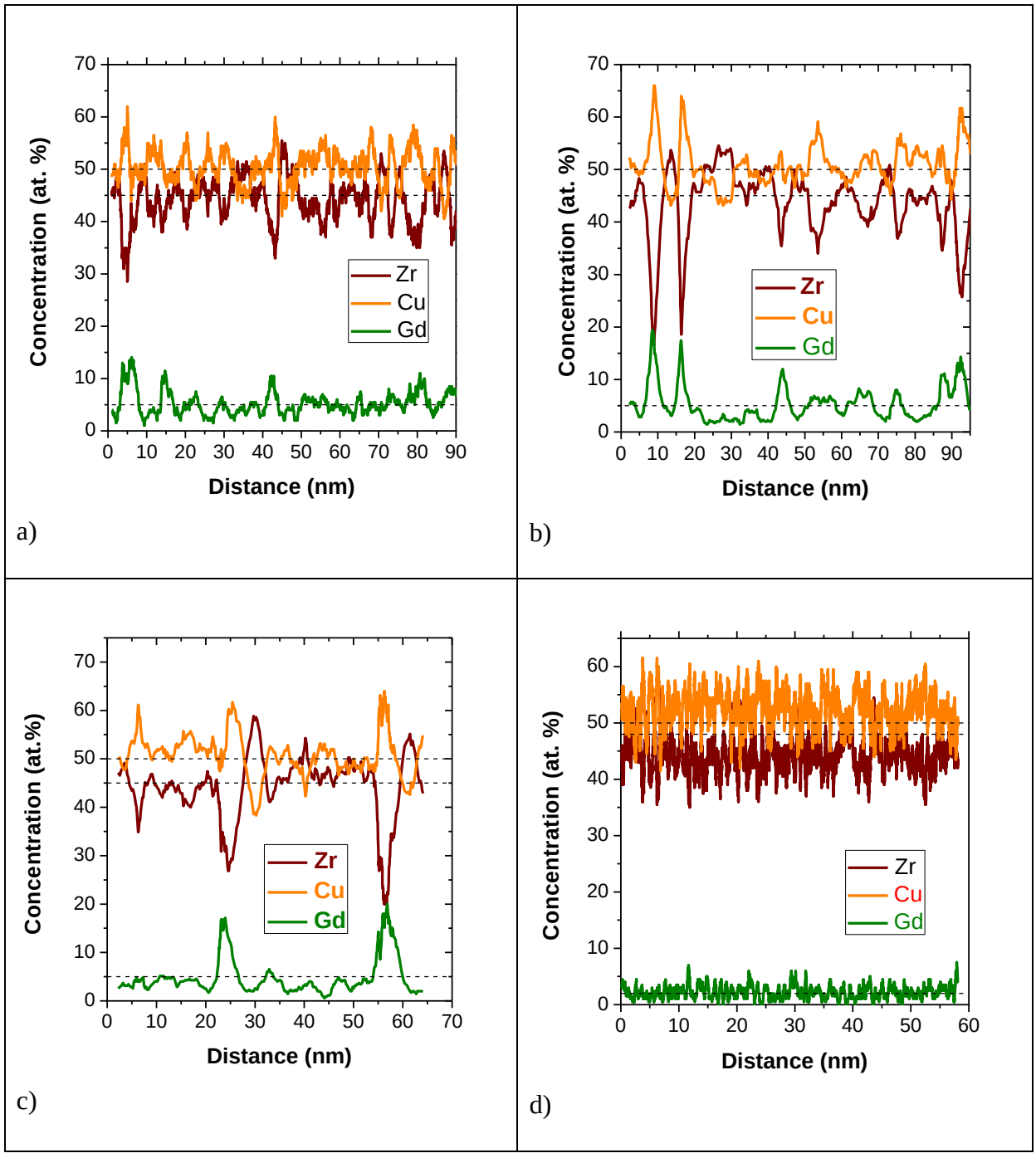

Figure 6: Composition profile along a selected cylinder of Figure 3 (2 nm in diameter). a) $Cu_{50}Zr_{45}Gd_5$: as-quenched state b) $Cu_{50}Zr_{45}Gd_5$: after annealing 673 K for 10 min (within super-cooled liquid state) c) $Cu_{50}Zr_{45}Gd_5$: after annealing 723 K for 10 min (above the crystallization temperature) d) $Cu_{50}Zr_{48}Gd_2$: as-quenched state. Fluctuations of the chemical composition with nanometer size are visible. Clusters are enriched in Gd and Cu. With annealing treatment the amplitude of the concentration fluctuations increases.

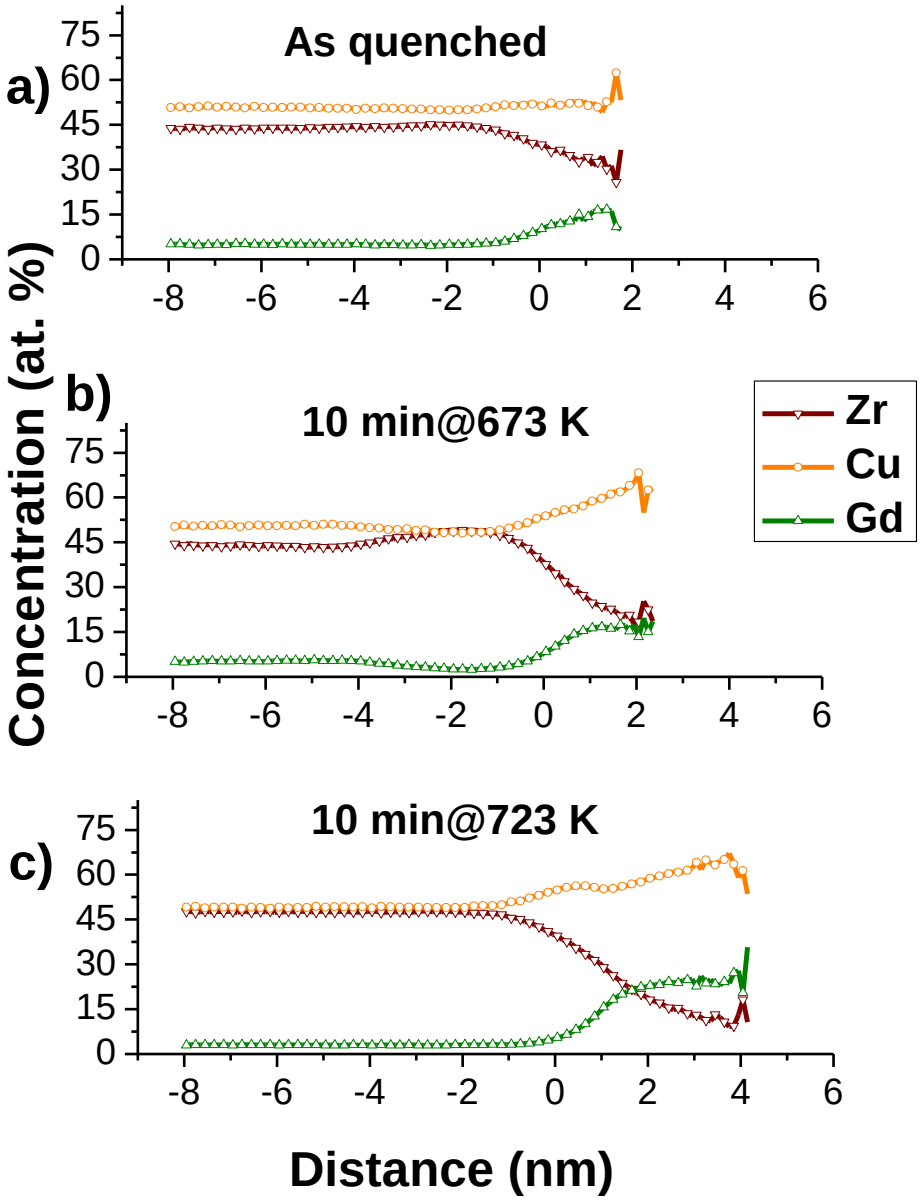

Figure 7: Proximity histograms for as-quenched (a) and annealed (b,c) $Cu_{50}Zr_{45}Gd_5$ glasses. A statistical average of the element compositions within the Gd-enriched clusters and their surrounding is presented from the analysis of more then 200 clusters. An up-hill diffusion of Gd and Cu atoms is seen by the comparison of the as-quenched state with the at 673 K annealed glass. The increase is accompanied by depletion of the elements from the surrounding of the cluster. Both give direct evidence of the spinodal character of the decomposition.

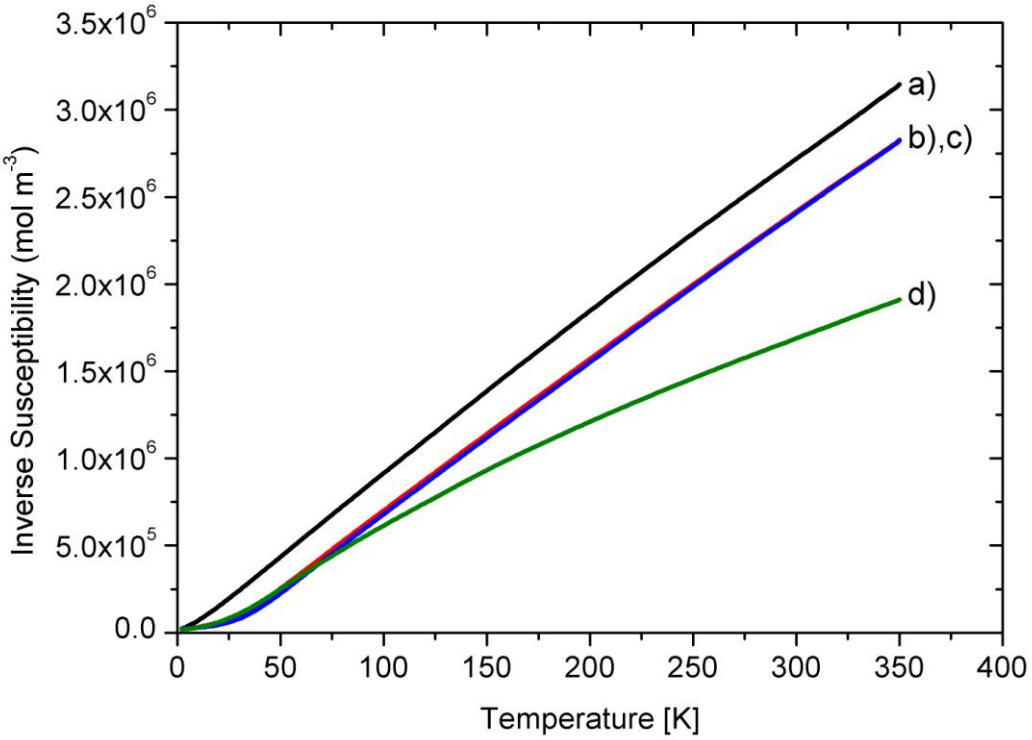

Figure 8: Inverse susceptibility versus temperature of a) $Cu_{50}Zr_{48}Gd_2$: as-quenched state, b) $Cu_{50}Zr_{45}Gd_5$: as-quenched state, c) $Cu_{50}Zr_{45}Gd_5$: after annealing 673 K for 10 min (within super-cooled liquid state), d) $Cu_{50}Zr_{45}Gd_5$: after annealing 723 K for 10 min (above the crystallization temperature). At low temperature the deviation from the linear dependence indicates the transformation from the paramagnetic state to ferromagnetism due to magnetic ordering within the Gd-enriched clusters.

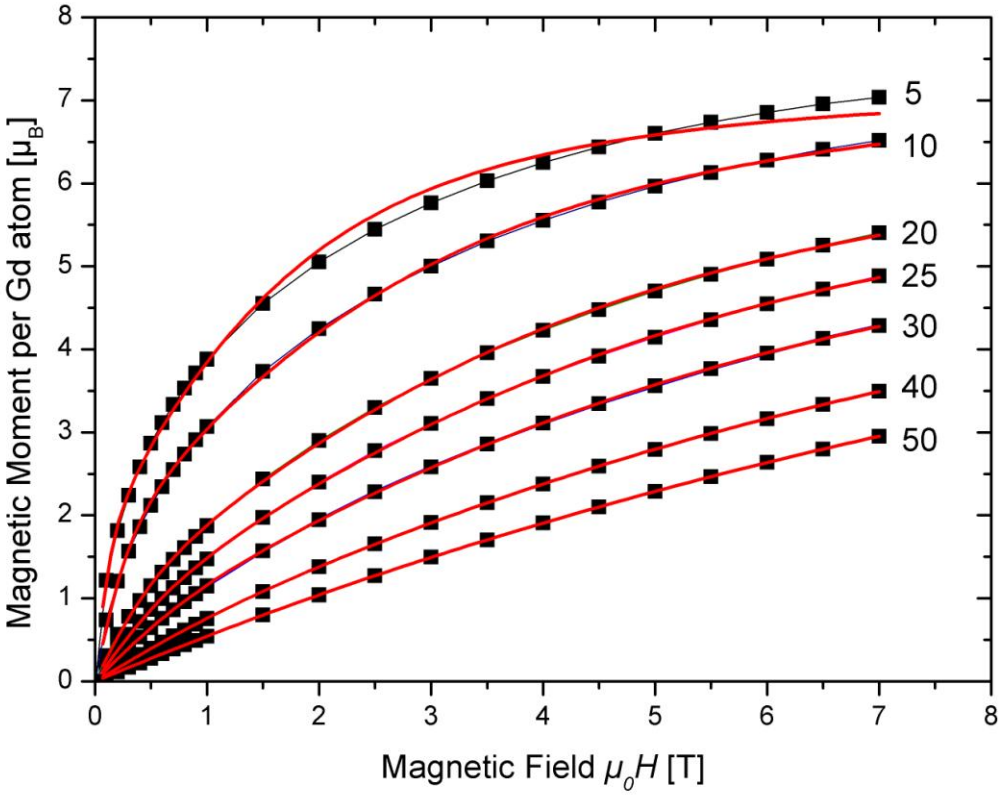

Figure 9: Magnetization versus applied field at low temperatures of as-quenched $Cu_{50}Zr_{45}Gd_5$ glass. The experimental data were fitted by a sum of two Brillion functions (solid lines) representing the magnetic contributions of the Gd atoms in the clusters, and those of the matrix respectively.

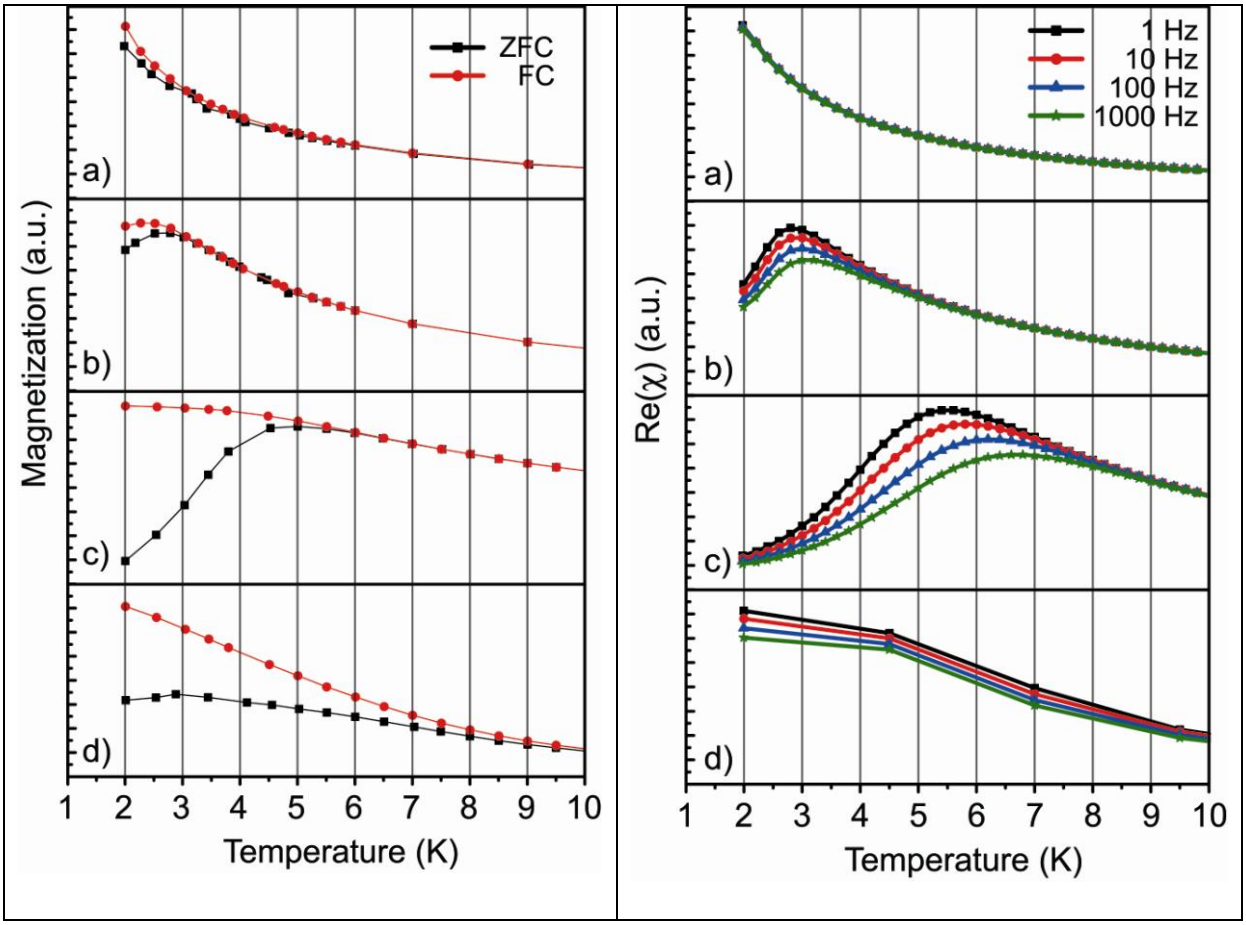

Figure 10 : Zero-field-cooled (ZFC) and Field-cooled (FC) magnetization measurements (left side) and ac-susceptibility's real part Re(χ) (right side) in the temperature range from 2 to 10 K for a) $Cu_{50}Zr_{48}Gd_2$: as-quenched state, b) $Cu_{50}Zr_{45}Gd_5$: as-quenched state, c) $Cu_{50}Zr_{45}Gd_5$: after annealing 673 K for 10 min (within super-cooled liquid state), d) $Cu_{50}Zr_{45}Gd_5$: after annealing 723 K for 10 min (above the crystallization temperature).

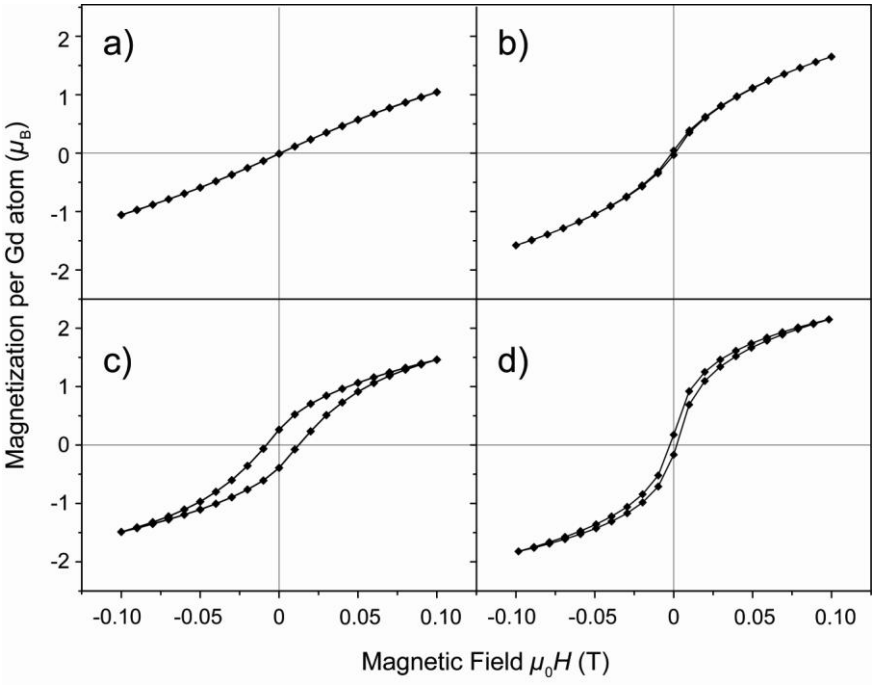

Figure 11: Magnetic Hysteresis Loops at 2 K for a) $Cu_{50}Zr_{48}Gd_2$: as-quenched state, b) $Cu_{50}Zr_{45}Gd_5$: as quenched state, c) $Cu_{50}Zr_{45}Gd_5$: after annealing 673 K for 10 min (within super-cooled liquid state), d) $Cu_{50}Zr_{45}Gd_5$: after annealing 723 K for 10 min (above the crystallization temperature).

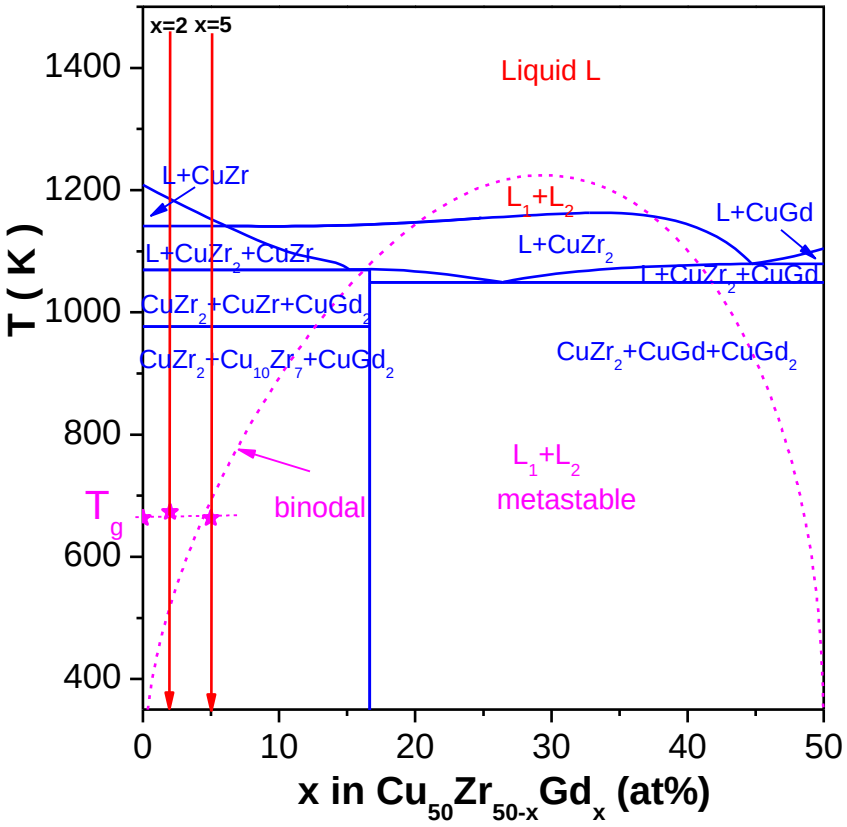

Figure 12: Pseudo-binary section $Cu_{50}Zr_{50}$-$Cu_{50}Gd_{50}$ of the Cu-Zr-Gd phase diagram. The temperature of liquid-liquid phase separation depends strongly on the composition as depicted by the bimodal curve.Different microstructures are obtained for rapidly quenched glasses as a consequence of the thermodynamic properties of the undercooled melts with respect to the glass transition temperature, $Cu_{50}Zr_{45}Gd_5$: $T_{crit} \approx T_g$, $Cu_{50}Zr_{48}Gd_2$: $T_{crit} < T_g$.

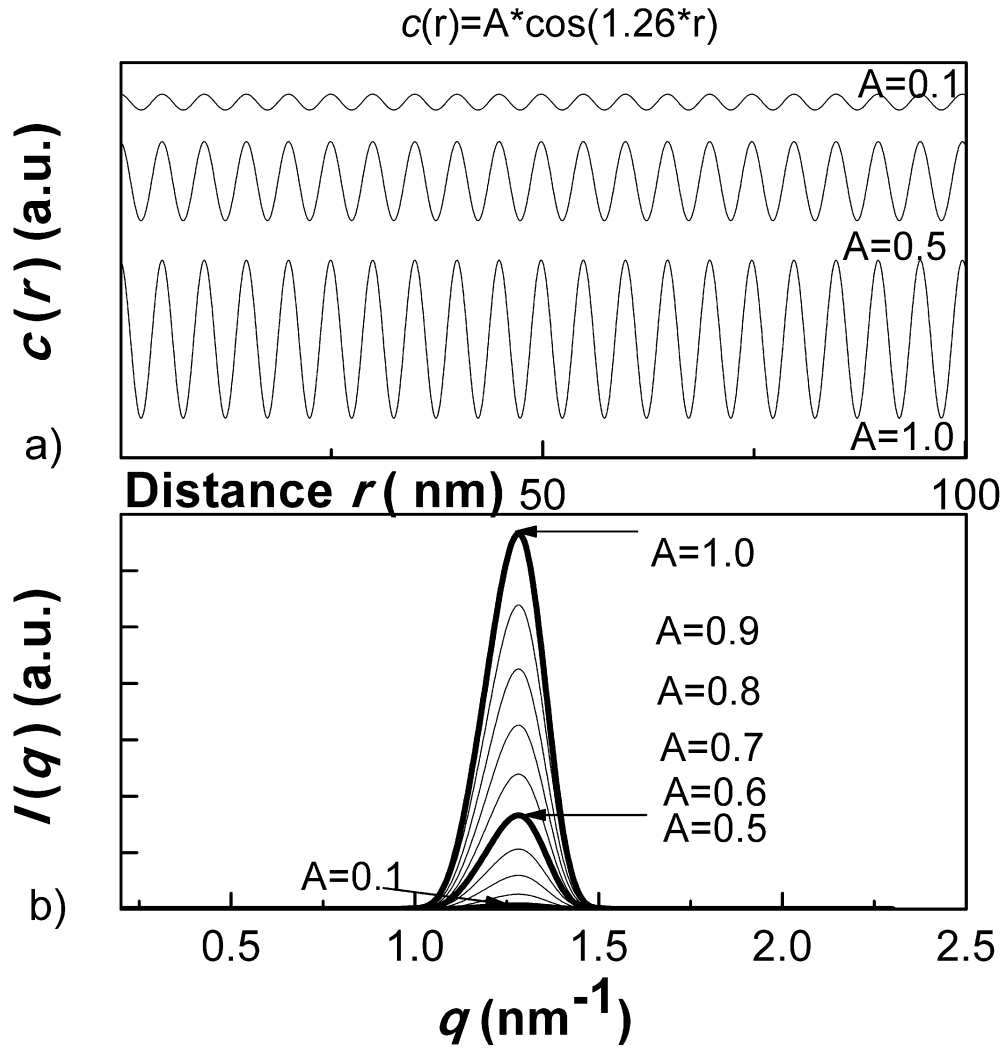

Figure 13: Schematic presentation of fluctuation in real space and corresponding diffraction in reciprocal space by a spinodal decomposition mechanism [16]: a) Concentration fluctuation $c(r)$ and b) corresponding SAXS intensity $I(q)$ as function of amplitude A.

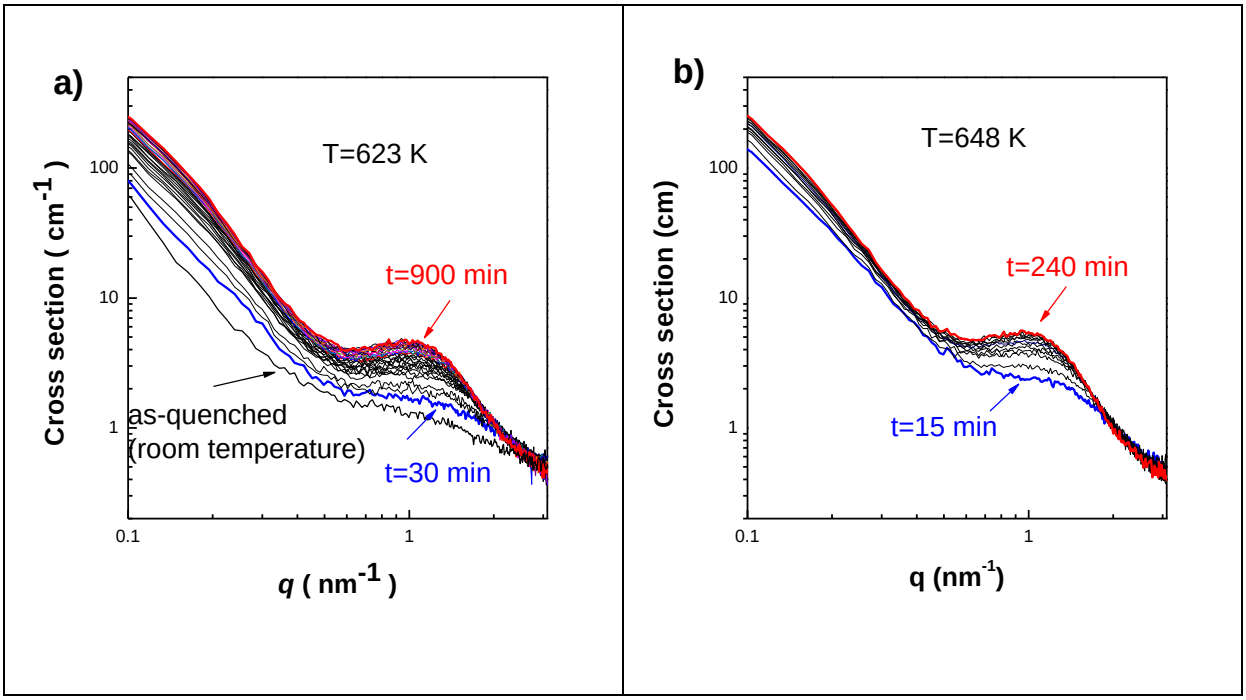

Figure 14: In situ SAXS measurement of $Cu_{50}Zr_{45}Gd_5$ glass at elevated temperatures, a) T= 623 K, b) T =648 K . Interference maximum at q=1.2 nm^{-1} increases in height with time pointing to spinodal mechanism

Tables

Table 1: Comparison of micostructural parameters calculated using proximity histograms

	as-quenched				10 min@673 K				10 min@723 K			
	Size (nm)	Cu	Zr	Gd	Size (nm)	Cu	Zr	Gd	Size (nm)	Cu	Zr	Gd
Cluster	**2.8**	51.9	34.1	14	**3.2**	59.4	25.1	15.5	**6.0**	60	17.3	22.7
Matrix		50.6	44.3	5.1		49.9	45.4	4.7		49.1	47.6	3.3
Cluster density	0.0009 nm^{-3}				0.0010 nm^{-3}				0.0002 nm^{-3}			

Table 2: Weiss constant Θ, minimum temperature $T_{p,min}$ down to which inverse susceptibilities obtained from the FC magnetization measurements show linear progression, effective magnetic moment μ_{eff}, magnetization $\mu_{2K,7T}$ at 2 K and at a magnetic field of 7 T, temperature T_f at which ac-susceptibility's real part at 1 Hz exhibits a maximum and its frequency shift $S_F = \Delta T_f / [T_f \Delta(\log \omega)]$ with varying frequency for $Cu_{50}Zr_{48}Gd_2$ and $Cu_{50}Zr_{45}Gd_5$ after various annealing treatments.

Sample	Θ (K)	$T_{p,min}$ (K)	μ_{eff} (μ_B)	$\mu_{2K,7T}$ (μ_B)	T_f (K)	$\Delta T_f / [T_f \Delta(\log\omega)]$
$Cu_{50}Zr_{48}Gd_2$ as prepared	7.0(1)	19(3)	7.83(1)	6.81(1)	-	-
$Cu_{50}Zr_{45}Gd_5$ as prepared	20.2(1)	48(3)	8.50(1)	7.24(1)	2.8(2)	0.033(2)
$Cu_{50}Zr_{45}Gd_5$ 673 K/10 min	23.4(1)	48(3)	8.42(1)	6.91(1)	5.4(2)	0.062(1)
$Cu_{50}Zr_{45}Gd_5$ 723 K/10 min	No paramagnetic region			6.85(1)	-	-

Table 3: Magnetic moments of the Gd-enriched cluster m^*_1 and matrix phase m^*_2 of $Cu_{50}Zr_{50-x}Gd_x$ glasses

		2K	5K	10K	20K	25K	30K	40K	50K
$Cu_{50}Zr_{45}Gd_5$ as quenched	$\boldsymbol{m}^*_1/7.9\mu_B$	43	18	16	18	17	17	15	13
	$\boldsymbol{m}^*_2/7.9\mu_B$	1	1	1.1	1.8	2.0	2.0	2.1	2.1
$Cu_{50}Zr_{45}Gd_5$ 673 K//10 min	$\boldsymbol{m}^*_1/7.9\mu_B$	43	32	36	42	35	29	20	26
	$\boldsymbol{m}^*_2/7.9\mu_B$	1	1	1.1	1.8	2.1	2.2	2.2	2.5
$Cu_{50}Zr_{48}Gd_2$ as quenched	$\boldsymbol{m}^*_1/7.9\mu_B$	1	7	4	4	5	8	6	20
	$\boldsymbol{m}^*_2/7.9\mu_B$	1	1	1	1.2	1.2	1.4	1.1	1.4

Graphical Abstract

Structural and Magnetic Nano-clusters in $Cu_{50}Zr_{50-x}Gd_x$ (x = 5 at%) Metallic Glasses

N. Mattern, A. Shariq, B. Schwarz, U. Vainio, J. Eckert

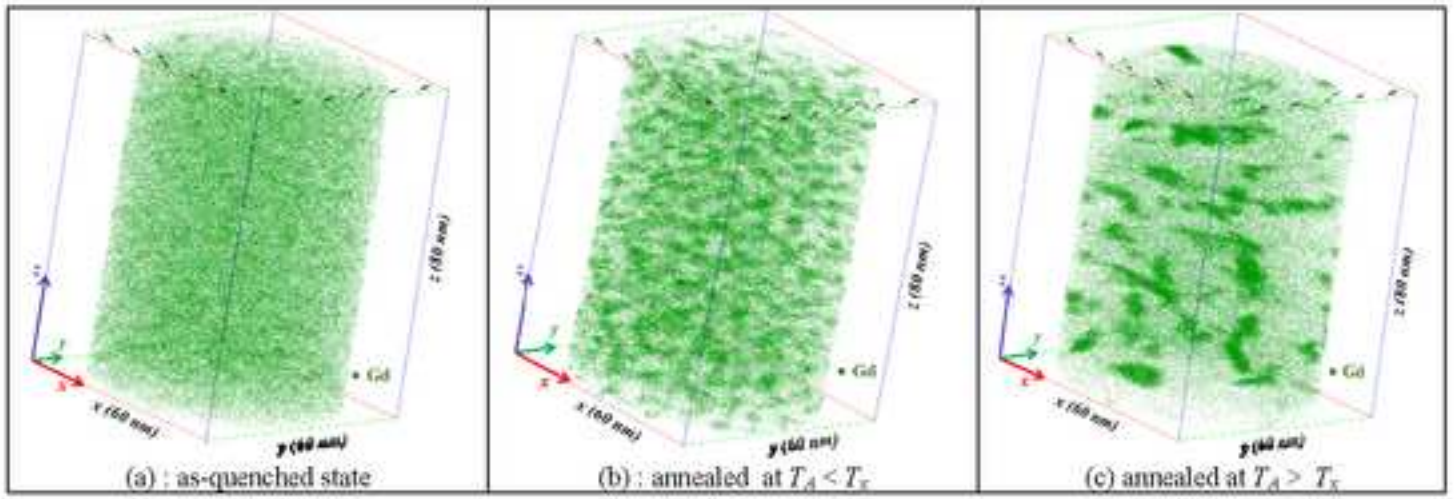

(a) : as-quenched state (b) : annealed at $T_A < T_x$ (c) annealed at $T_A > T_x$

Phase separated metallic glasses consisting of Gd-enriched clusters of 2 nm size are formed upon rapid quenching $Cu_{50}Zr_{45}Gd_5$ melt as shown by the spatial distribution of the Gd atoms measured by atom probe tomography (a). Annealing in the glassy or supercooled liquid state leads to an increase of concentration fluctuations pointing to spinodal decomposition as mechanism (b). Ostwald type ripening on a nanoscale is observed as first stage of crystallization (c). The Gd-enriched clusters exhibit ferromagnetic ordering below 50 K.